Journal of Statistical Mechanics:
Theory and Experiment

Entanglement Hamiltonian in the non-Hermitian SSH model

OPEN ACCESS

Journal of Statistical Mechanics: Theory and Experiment
An IOP and SISSA journal

PAPER: Quantum statistical physics, condensed matter, integrable systems

Entanglement Hamiltonian in the non-Hermitian SSH model

Federico Rottoli[1,3,*], **Michele Fossati**[1] **and Pasquale Calabrese**[1,2]

[1] SISSA and INFN Sezione di Trieste, via Bonomea 265, 34136 Trieste, Italy
[2] ICTP, Strada Costiera 11, 34151 Trieste, Italy
[3] Dipartimento di Fisica dell'Università di Pisa, Largo Pontecorvo 3, 56127 Pisa, Italy
E-mail: frottoli@sissa.it

Received 14 February 2024
Accepted for publication 29 April 2024
Published 10 June 2024

Online at stacks.iop.org/JSTAT/2024/063102
https://doi.org/10.1088/1742-5468/ad4860

Abstract. Entanglement Hamiltonians provide the most comprehensive characterisation of entanglement in extended quantum systems. A key result in unitary quantum field theories is the Bisognano-Wichmann theorem, which establishes the locality of the entanglement Hamiltonian. In this work, our focus is on the non-Hermitian Su-Schrieffer-Heeger (SSH) chain. We study the entanglement Hamiltonian both in a gapped phase and at criticality. In the gapped phase we find that the lattice entanglement Hamiltonian is compatible with a lattice Bisognano-Wichmann result, with an entanglement temperature linear in the lattice index. At the critical point, we identify a new imaginary chemical potential term absent in unitary models. This operator is responsible for the negative entanglement entropy observed in the non-Hermitian SSH chain at criticality.

Keywords: entanglement entropies, entanglement in extended quantum systems, quantum criticality

*Author to whom any correspondence should be addressed.

Contents

1. Introduction

In recent years, the study of entanglement has attracted a lot of interest from several different communities and has emerged as a unifying theme across quantum physics, in fields ranging from quantum information [1] and high energy physics [2], to statistical mechanics [3–5] and condensed matter physics [6]. Given a pure state described by the density matrix $\rho = |\Psi\rangle\langle\Psi|$ and considering a bipartition of the system in A and B, the information about the entanglement between the two subsystems is encoded in the reduced density matrix, obtained by tracing over the Hilbert space of one of the two subsystems

$$\rho_A = \mathrm{Tr}_B\, \rho. \tag{1}$$

If the density matrix ρ is entangled, then the reduced density matrix in equation (1) corresponds to a mixed state and the von Neumann and Rényi entropies of ρ_A [7, 8]

$$S_A = -\,\mathrm{Tr}\,[\rho_A \log \rho_A]\,, \qquad S_A^{(n)} = \frac{1}{1-n} \log \mathrm{Tr}\, \rho_A^n. \tag{2}$$

are good entanglement monotones. The knowledge of all the Rényi entropies allows in turn to compute the full entanglement spectrum, i.e, the spectrum of the reduced density matrix [9–11].

While the entanglement entropies in equation (2) are very useful, they do not entirely capture the entanglement properties of the system. Over the years, more comprehensive characterisations, beyond what can be exclusively derived from the knowledge of the

J. Stat. Mech. (2024) 063102

entanglement spectrum, have been investigated. Arguably, the most complete understanding stems from the entanglement (or modular) Hamiltonian (EH), which is the logarithm of the (normalised) reduced density matrix [12–14]

$$\rho_A = \frac{e^{-K_A}}{Z_A}. \tag{3}$$

This operator contains much more information than the entanglement entropies, since, unlike the latter, its specific form depends not only on the eigenvalues but also on the eigenvectors of ρ_A.

Although calculating the EH is considerably more challenging than determining the entanglement entropies, a rich theoretical framework has been developed during the last decades. The most remarkable result is the Bisognano-Wichmann theorem [12–16]. Considering the vacuum state of a unitary relativistic quantum field theory (QFT) on $\mathbb{R}^{d+1}$ and taking as subsystem the half-space $x^1 > 0$, the Bisognano-Wichmann theorem asserts that the EH in the half-space is the generator of Lorentz boosts

$$K_A = 2\pi \int_{x^1>0} \mathrm{d}^d x\, x^1\, T_{00}(x)\,, \tag{4}$$

where $T_{00}(x)$ is the energy density. This result is remarkable for several reasons. First, it is extremely general, holding for all unitary Lorentz invariant QFTs, independently of the dimension of space-time and of the mass spectrum. Another significant property is the fact that the EH in equation (4) has a local structure, given by the integral of local operator with a linearly increasing local entanglement temperature $\beta(x) = x^1$. Finally, the Bisognano-Wichmann theorem provides a mathematical proof of the Unruh effect [17–19], as discussed in [12–14].

For generic massive QFTs, the Bisognano-Wichmann theorem in equation (4) is the only known analytic result. For conformal field theories (CFT), instead, the extended symmetry makes it possible to obtain more general results. In particular, the Hislop-Longo theorem [12, 20] (see also [21–23]) provides the EH of the ground state of a CFT in any ball shaped region. Even more general results can be obtained in $1+1$-dimensional unitary CFTs, where the infinite dimensional Virasoro symmetry allows one to map the Bisognano-Wichmann result in equation (4) in several different geometries [22, 23]. In particular, for the conformal vacuum state, if the subsystem is a single interval ($A = [0, \ell]$) the EH takes the form [20–23]

$$K_A = 2\pi \int_0^\ell \mathrm{d}x\, \beta(x)\, T_{00}(x)\,, \qquad \text{with } \beta(x) = \frac{x\,(\ell - x)}{\ell}\,, \tag{5}$$

a formula that inherits the local structure of the Bisognano-Wichmann result, with a parabolic local entanglement temperature $\beta(x)$. We remark that this local structure is very peculiar and it fails to hold as soon as we consider minor modifications such as for the lowest excited states [24] and when considering multiple intervals [25, 26]. This property is not only of theoretical interest, but recently in [27–31] it has been leveraged

J. Stat. Mech. (2024) 063102

to efficiently construct in synthetic quantum systems the ground state of lattice models using a variational approach.

A separate line of research, yielding numerous results, concerns the study of the EH in unitary $1+1$-dimensional integrable lattice models [32–47]. In these systems, the EH of the ground state in the half-space $x>0$ is intimately related to Baxter's corner transfer matrix (CTM) $\widehat{A}$ [48–50]. Considering, for example, isotropic square lattices, the effect of the CTM is to add a full angular segment to a piece of lattice, mapping a horizontal row to a vertical one and vice versa. Using this property it is possible to show that the lattice reduced density matrix in the half-line can be expressed as the product of four CTMs [7, 35, 51]

$$\rho_A = \frac{\widehat{A}^4}{\operatorname{Tr}\widehat{A}^4}, \tag{6}$$

where $Z = \operatorname{Tr}\widehat{A}^4$ is the partition function. Recalling the definition (3) of the EH, equation (6) implies that it is proportional to the logarithm of fourth power of the CTM [35]

$$K_A = -\log \widehat{A}^4. \tag{7}$$

This correspondence between EHs and CTMs has made it possible to obtain the EHs in several integrable models. It has been observed that in certain integrable models, the logarithm of the CTM and the EH can be written in terms of the density of the lattice Hamiltonian h_j with a linearly increasing local temperature

$$K_A \propto \sum_{j=0}^{\infty} j\, h_j\,, \tag{8}$$

with a non-trivial proportionality constant. This behaviour has been identified in various spin systems such as the Ising model [33–35], the XXZ [36, 37, 48], the XYZ chains [38–40], the anisotropic XX chain [43], and in bosonic models such as the harmonic chain [41–43]. Comparing equation (8) with the Bisognano-Wichmann theorem in equation (4), it is evident that the two EHs share the same structure. In fact, the connection between the two results runs deeper than a superficial similarity. Tetel'man [38] and Itoyama and Thacker [39, 52–54] independently showed that in these integrable models the logarithm of the CTM is the generator of a continuous group of lattice Lorentz transformations, akin to the role played by the generator of Lorentz boosts in the Bisognano-Wichmann theorem.

Despite the wealth of results for unitary models, nothing is known for non-Hermitian theories. In particular, since one of the hypothesis of the Bisognano-Wichmann theorem (4) is that the Hilbert space carries a unitary representation of the Poincaré group [12, 15, 16], it is not obvious how to adapt to non-unitary CFTs this theorem and its corollary (5). Non-Hermitian models [55, 56] have recently attracted a lot of interest for several reasons, including but not restricted to the study of the PT-symmetric systems

J. Stat. Mech. (2024) 063102

[57–62], optical phenomena [63, 64] and the study of open systems [65–67] and measurement induced transitions [68–72]. It is then very natural to explore the entanglement properties within this class of systems.

A pioneering study was carried out in [73], where the authors have studied the entanglement entropy and the entanglement spectrum in the non-Hermitian Su-Schrieffer-Heeger (SSH) model at criticality (reviewed in section 2). Remarkably, it was observed that the entanglement entropies obey the logarithmic dependence on the subsystem length typical of critical systems [7, 74], but with a negative central charge $c = -2$ (see also [75]). Later, in [76], the analysis has been extended to the symmetry resolved entanglement entropies. In this work we move a step further, conducting an exploratory and thorough numerical investigation of the EH in the non-Hermitian SSH model, both in the gapped phase and at criticality. In the gapped phase we observe that the lattice EH has a structure analogous to the one of integrable lattice models reported in equation (8). At the critical point, we instead find an additional term not accounted for in the Bisognano-Wichmann corollary in equation (5), which is responsible for the negativeness of the entanglement entropies.

The present manuscript is organised as follows. First, in section 2 we review the non-Hermitian SSH model, with particular focus on the non-unitary $c = -2$ bc-ghost CFT which describes the critical point. In section 3 we report the main results of this work, the numerical lattice EH in the non-Hermitian SSH model. We first consider the topologically trivial gapped phase in section 3.1 and we then study the critical point in section 3.2. We draw our conclusions in section 4.

2. The non-Hermitian Su–Schrieffer–Heeger model

Before presenting our results, in this section we review the non-Hermitian model that we study in this paper. We consider the non-Hermitian SSH (nH-SSH) chain with PT-symmetry on a discrete circle of $L = 2N$ sites, described by the Hamiltonian

$$H = \sum_{j\in\mathbb{Z}_N} \left(-w\, c^\dagger_{2j} c_{2j+1} - v\, c^\dagger_{2j-1} c_{2j} + \text{h.c.} \right) + \mathrm{i}u \sum_{j\in\mathbb{Z}_N} \left(c^\dagger_{2j} c_{2j} - c^\dagger_{2j+1} c_{2j+1} \right), \quad (9)$$

with $u, v, w > 0$. A schematic representation of this Hamiltonian is depicted in figure 1. We assume quasi-periodic boundary conditions, i.e. $c_{j+L} = e^{\mathrm{i}\delta} c_j$, with $0 < \delta \ll 1$. The reason for this choice will be explained later. The model is a fermionic chain with nearest neighbours hoppings, which have alternating strength on even–odd links. The staggered imaginary chemical potential breaks the hermiticity of the Hamiltonian. Notice that our conventions match those in [75] after setting $v_1 = 0$ and $v_2 = v$ and identifying their up (down) sites with our even (odd) ones.

The Hamiltonian becomes block diagonal after a Fourier transform of the lattice operators, performed separately on the even and odd sites

$$\tilde{c}_{k,\mathrm{e}} = \frac{1}{\sqrt{N}} \sum_{j\in\mathbb{Z}_N} e^{-\mathrm{i}kj} c_{2j}\,, \qquad \tilde{c}_{k,\mathrm{o}} = \frac{1}{\sqrt{N}} \sum_{j\in\mathbb{Z}_N} e^{-\mathrm{i}kj} c_{2j+1}\,, \quad (10)$$

J. Stat. Mech. (2024) 063102

Figure 1. Schematic representation of the nH-SSH model, described by equation (9). The nearest neighbours hoppings have alternating strengths v and w. The imaginary chemical potential is set to $\mathrm{i}u$ on the even sites and $-\mathrm{i}u$ on the odd sites.

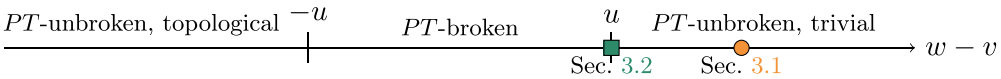

Figure 2. Phase diagram of the nH-SSH model, explained in the main text. The orange circle and the green square mark the points in parameter space for which we study the EH, reported in sections 3.1 and 3.2 respectively.

with

$$k \in \frac{2\pi}{N}\left(\mathbb{Z}_N + \frac{\delta}{2\pi}\right), \tag{11}$$

where the shift in momentum space is due to the δ-twisted boundary conditions. The Hamiltonian then becomes

$$H = \sum_k \begin{pmatrix} \tilde{c}^\dagger_{k,\mathrm{e}} & \tilde{c}^\dagger_{k,\mathrm{o}} \end{pmatrix} \begin{pmatrix} \mathrm{i}u & -w - ve^{-\mathrm{i}k} \\ -w - ve^{\mathrm{i}k} & -\mathrm{i}u \end{pmatrix} \begin{pmatrix} \tilde{c}_{k,\mathrm{e}} \\ \tilde{c}_{k,\mathrm{o}} \end{pmatrix}, \tag{12}$$

and the eigenvalues of the matrix in equation (12) are the single-particle energies.

Varying the relative strengths of the parameters u, v, w, the model admits three different gapped phases [73]. If $v - w \in (-u, u)$, the PT symmetry is broken so that the energy spectrum is complex and the eigenvalues appear in complex conjugate pairs. In the two phases $v - w > u$ or $v - w < -u$, the PT symmetry is unbroken and the energy spectrum is real. The latter two phases are distinguished by topological properties, as discussed in [77]. The resulting phase diagram is given in figure 2.

Two critical points occur for $v - w = \pm u$. In these cases, the single-particle spectrum is $\epsilon_{\pm,k} = \pm\sqrt{2vw(1+\cos k)}$ and the gap closes at $k = \pi$, leading locally to a linear spectrum with speed of sound

$$c_S = \sqrt{vw}. \tag{13}$$

Moreover, at $k = \pi$ the kernel of the Hamiltonian (12) is not diagonalisable, as it is made of a 2×2 Jordan block. This is called an exceptional point in momentum space. The exceptional point occurs because, as $k \to \pi$, the two eigenspaces become more and more collinear, and they perfectly coincide at $k = \pi$.

https://doi.org/10.1088/1742-5468/ad4860

J. Stat. Mech. (2024) 063102

Finally, since the Hamiltonian is a linear combination of terms of the form $c_i^\dagger c_j$, it is invariant under the $U(1)$ generated by

$$Q = \sum_{j \in \mathbb{Z}_{2N}} c_j^\dagger c_j \,. \tag{14}$$

In this paper, we will investigate the ground-state of the system in the PT-unbroken trivial phase and the critical point between the PT-unbroken trivial phase and the PT-broken phase, marked in figure 2 with a orange circle and a green square, respectively. In [73], the latter point has been identified with the fermionic bc-ghost CFT with central charge $c = -2$, which we review in the following section.

2.1. *bc*-ghost CFT

The bc-ghost CFTs are a family of theories governed by the following action [78–82]

$$S = \int \mathrm{d}^2 z \left(b\,\bar{\partial} c + \bar{b}\,\partial \bar{c} \right), \tag{15}$$

where b and c are anticommuting holomorphic fields and $\bar{b}$ and $\bar{c}$ are the corresponding anti-holomorphic fields. The different members of this family are distinguished by the value of the central charge and by the conformal dimension of the fields c and b. In particular, the CFT which describes the nH-SSH critical point is the one with central charge $c = -2$ [73], in which the fields have conformal weight $h_b = 1, h_c = 0$. All these theories have a conserved current $J =: cb:$ so that the field c has charge 1 and b has charge -1, independently of the specific realisation and central charge.

The CFT with $c = -2$ is one of the simplest instances of a logarithmic CFT [80], incorporating reducible but not indecomposable representations of the Virasoro algebra. Specifically, the fields c and the identity field share the same conformal weights, leading to the formation of a 2-dimensional Jordan block in the Virasoro modes L_0 and $\bar{L}_0$. This phenomenon occurs exclusively in the untwisted sector of the theory, which corresponds to periodic boundary conditions on a cylinder. In the scenario where δ-twisted boundary conditions are adopted, the fields acquire a phase factor $e^{\mathrm{i}2\pi\delta}$ as they move around the non-contractible loop of the cylinder. Consequently, the identity field is no longer part of the spectrum, and the system's ground state becomes associated with the twist field σ_δ [80]. The conformal dimension of σ_δ is given by $h_{\sigma_\delta} = \delta(\delta - 1)/2$, which is negative for $\delta \neq 0$. This implies that for $\delta \neq 0$, there is no Jordan block for L_0 and $\bar{L}_0$, effectively eliminating the logarithmic singularities. It is noteworthy that the presence of the Jordan block in periodic boundary conditions and its absence in the twisted sectors draws a further analogy with the nH-SSH model.

2.2. Left-right ground-state

Before concluding this brief review, we would like to emphasise the states that are the focus of this paper. First, in both of the cases we consider (see figure 2), the Hamiltonian has a real spectrum, thus there is a well defined notion of a ground state as the eigenstate with minimum energy eigenvalue. We denote by $|R\rangle$ the right ground state of the

J. Stat. Mech. (2024) 063102

Hamiltonian, defined by $H|R\rangle = E_{\rm gs}|R\rangle$, while we denote with $\langle L|$ the left ground-state, defined by $\langle L|H = E_{\rm gs}\langle L|$. Since the Hamiltonian is non-Hermitian, the left ground state is not the 'bra' of the right ground state, in other words, $|L\rangle \neq |R\rangle$.

We consider the density matrix $\rho = |R\rangle\langle L|$, which we call the left-right ground state [73, 75, 76, 83–87]. Indeed, this can be seen as the zero-temperature limit of the thermal state $e^{-\beta H}/Z$ and therefore is the most natural object to be studied in field theory. The density matrix ρ is positive semi-definite but not Hermitian and therefore the reduced density matrix ρ_A is not positive semi-definite. This means that the entanglement entropy between a subsystem and its complement can be negative. Indeed, the entanglement entropy scales as $c/3\log\ell$, with $c = -2$ [73].

The symmetry-resolved entanglement, relative to the $U(1)$ symmetry (14), at the critical point has been studied in [76]. Of relevance for this paper, it has been understood that the eigenvalues of the reduced density matrix are either positive or negative depending on the sign of the charge sector, namely $\operatorname{sign}\lambda_q = (-1)^{q-\langle Q_A\rangle}$, where λ_q stands for an eigenvalue of ρ_A in the charge sector q of Q_A (i.e. the charge (14) restricted to A). We will show in section 3.2 that we can identify the source of this behaviour in the form of the EH.

2.3. Correlation function

A key object in the analysis of the EH of the left-right ground state is the two-point correlation matrix C with entries [73, 76]

$$C_{2j+a,2l+b} = \langle L|c^\dagger_{2j+a}c_{2l+b}|R\rangle = \frac{1}{N}\sum_k e^{-{\rm i}k(j-l)}\mathcal{G}(k)_{ab}\,, \quad a,b\in\{0,1\}\,, \tag{16}$$

with

$$\mathcal{G}(k) = \frac{1}{2}\begin{pmatrix} 1-\cos(2\xi_k) & -\sqrt{\frac{\eta_k^*}{\eta_k}}\sin(2\xi_k) \\ -\sqrt{\frac{\eta_k}{\eta_k^*}}\sin(2\xi_k) & 1+\cos(2\xi_k)\end{pmatrix}, \tag{17}$$

where $2\xi_k = \tan^{-1}(|\eta_k|/(i\,u))$, $\eta_k = -w - ve^{-ik}$. Due to the dimerization of the hopping amplitudes v, w, the correlation matrix C presents a block structure. In the thermodynamic limit $L\to\infty$, C is a block Toeplitz matrix generated by the symbol $\mathcal{G}$.

3. Lattice entanglement Hamiltonians of the non-Hermitian SSH model

This section contains the main results of this paper, the numerical lattice EH in the non-Hermitian SSH model and an analytic conjecture for its behaviour. In order to compute numerically the lattice EH we use the known relation between fermionic Gaussian states

J. Stat. Mech. (2024) 063102

and the correlation matrix. Notice first that since the Hamiltonian (9) is quadratic, the ground state is Gaussian [73, 76] and the reduced density matrix can be written as

$$\rho_A = \frac{1}{Z_A} \exp\left\{ - \sum_{i,j\in A} c_i^\dagger k^A_{i,j} c_j \right\}, \tag{18}$$

where $k^A_{i,j}$ is the kernel of the EH, i.e. the single-particle EH. For Gaussian states as in equation (18), the kernel k^A can be obtained from the knowledge of the reduced correlation matrix, i.e. the matrix (16) with indexes restricted to A, $(C_A)_{i,j} = (C)_{i,j\in A}$. Using Peschel's formula [88–90] one has

$$k^A = \log\left[C_A^{-1} - \mathbb{I}\right]^{\mathrm{T}}, \tag{19}$$

where T denotes the matrix transpose. While equation (19) was initially derived for Hermitian models, as discussed in [73, 76], it remains valid in the non-Hermitian one under consideration. In [73, 76] the restricted correlation matrix of the non-Hermitian SSH model is used for the computation of the entanglement spectrum and the entropies. In the following we will compute the kernel of the EH using the correlation matrix (16).

We remark that the numerical computation of the formula (19) suffers from numerical instabilities and must be conducted at high precision. The reason for this instability is that many eigenvalues of the correlation matrix C_A are arbitrarily close to 0 and 1, and as a consequence the matrix inside of the logarithm in equation (19) has eigenvalues which are very close to 0 or very large. In our study we used the `python` library `mpmath` [91] and the software `Mathematica`, keeping up to 500 digits.

In rest of this section, we present the results for the EH of an interval $A = [0, \ell]$ in the left-right ground state. We first study the topologically trivial gapped phase $w - v > u$ with periodic boundary conditions and we compare with the known results in unitary integrable lattice models [43]. We then consider the critical point $w - v = u$ with a small twisting of the boundary conditions $\delta = 10^{-7}$, which as we explained in section 2 is described by the $c = -2$ bc-ghost CFT. We compare the results with the continuum prediction from unitary CFTs and we use our observations to formulate a conjecture for the EH of an interval in the ground state of the bc-ghost theory.

3.1. Entanglement Hamiltonian in the trivial gapped phase

Before studying the non-Hermitian model, it is instructive to first recall the known results in unitary gapped lattice models, in order to compare them with ours. As we reported in equation (8) in section 1, in certain integrable models the EH in the half-space follows the structure recognised by Tetel'man, Itoyama and Thacker, i.e. the EH is proportional to the Hamiltonian density with a local temperature equal to the lattice site, analogous to a lattice Bisognano-Wichmann behaviour [14, 38, 39, 49, 50, 52]. If we instead consider a finite interval, in the general case there are very few known analytic results. If the gap is sufficiently large, however, in [43] it was observed via numerical computations that near the two endpoints of the interval the EH follows the half-space

J. Stat. Mech. (2024) 063102

result of equation (8), only deviating from this behaviour in the middle of the interval, which give rise to a characteristic triangular entanglement temperature.

This triangular behaviour has been observed in several Hermitian models, such as the Hermitian SSH model (or dimerised hopping chain) and the harmonic chain [43]. Its physical interpretation is that, for short-range correlated systems, the EH density is affected only by the closest boundary, as the contribution from the furthest one is exponentially suppressed. Then the EH density behaves as the one of a semi-infinite subsystem (see equation (8)) and the RDM effectively factorises [92]. This argument is independent of unitarity and holds also for the non-hermitian model under consideration. It is therefore natural to wonder if this factorisation holds also for the non-Hermitian model under study.

Another important consequence of equation (8) is that in unitary lattice integrable modes, the half-space lattice EH does not couple fermions at distances larger than those in the corresponding lattice Hamiltonian. Correspondingly, within an interval, it was noted that near the endpoints, the EH does not exhibit higher couplings, only manifesting them in the crossover region at the center [43].

Let us now consider the non-Hermitian SSH model. Assuming that the structure of the EH in equation (8) holds also for this theory, from the Hamiltonian in equation (9) we can conjecture that the half-space lattice EH takes the form

$$K_A \propto \sum_{j=0}^{+\infty} \Big[(2j)w \left(c^\dagger_{2j} c_{2j+1} + c^\dagger_{2j+1} c_{2j} \right) + (2j+1) v \left(c^\dagger_{2j-1} c_{2j} + c^\dagger_{2j} c_{2j-1} \right) + \mathrm{i} \left(2j + \frac{1}{2} \right) u\, c^\dagger_{2j} c_{2j} - \mathrm{i} \left(2j + \frac{3}{2} \right) u\, c^\dagger_{2j+1} c_{2j+1} \Big], \tag{20}$$

with some unknown proportionality constant. Since we cannot access numerically the full EH of the half-space, in order to test the conjecture in equation (20) we study the EH of an interval $[0, \ell]$ in a finite system of length $L \gg \ell$. In analogy with the unitary case, we expect that for a sufficiently large gap, near the endpoints the EH will follow the half-space result in equation (20), with a crossover in the middle of the interval, giving rise to the typical triangular shape.

In figure 3 we report the results of the numerical calculation of the lattice EH in the gapped phase, for an interval of length $\ell = 100$ in a system of total length $L = 2000$ with periodic boundary conditions. We fix the parameters $v = u = 1$ and we study different gaps by varying the value of w, in particular we take $w = 5, 10$ and 20. The plots report the ratio between the kernel of the EH, k^A, obtained from equation (19) and the one of the Hamiltonian h in equation (9) as a function of the lattice site. On the left, in figure 3(b) we report the real part of the nearest-neighbour coupling $k^A_{j,j+1}$, divided by $(-w)$ for j even (circles) and by $(-v)$ for j odd (crosses). Dividing by these coupling constants, we isolate the entanglement temperature, which is expected to follow the triangular shape (see equation (20) and discussion below). Indeed we see that, apart from a small crossover region in the center of the interval, the nearest-neighbour coupling follows the expected behaviour for all values of w that we considered. This behaviour

https://doi.org/10.1088/1742-5468/ad4860

J. Stat. Mech. (2024) 063102

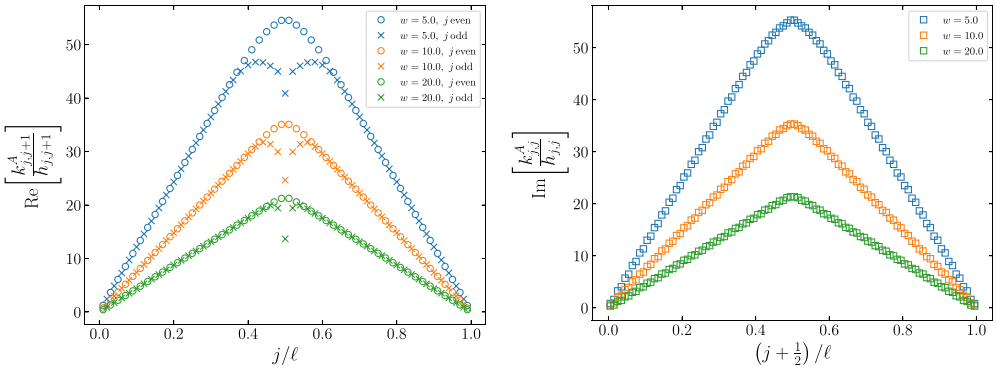

(a) Real part of the nearest-neighbour coupling $k^A_{j,j+1}$. **(b)** Imaginary part of the chemical potential $k^A_{j,j}$.

Figure 3. Entanglement temperature in the gapped phase $w - v > u$. In both plots we fix $v = u = 1$ and we consider different values of $w = 5, 10$ and 20 and we take a subsystem of length $\ell = 100$ in a full system of total length $L = 2000$. In the left plot we report, as a function of j/ℓ, the real part of the ratio of the nearest-neighbour EH coupling $k^A_{j,j+1}$ with the coupling $(h_{j,j+1})$, i.e. $-w$ for even j (circles) and $-v$ for odd j (crosses). The purpose of this ratio is to isolate the entanglement temperature. Apart from a small region in the center of the interval, the ratio follows the expected triangular shape (see discussion below equation (20)). In the right plot we report the imaginary part of the ratio between the staggered imaginary chemical potential $k^A_{j,j}$ with $+u$ $(-u)$ for even (odd) site j. Again, up to a small finite size oscillation, the ratio follows the predicted triangular shape.

is completely analogous to what observed in [43] for the dimerised hopping chain. The novel result is reported in the right plot, in figure 3(b), where we show the staggered imaginary chemical potential $k^A_{j,j}$, divided by u for j even and by $(-u)$ for j odd. Again, the role of this division is to isolate the entanglement temperature, which should agree with the one obtained from the nearest-neighbour coupling. Indeed we observe that, apart from a small oscillation due to finite size effects, the imaginary chemical potential follows the same triangular shape as the nearest-neighbour coupling, as expected from our conjecture in equation (20).

As a further check, in figure 4 we report the matrix plots of the real (left plot) and of the imaginary parts (right plot) of the single-particle EH k^A. According to our conjecture in equation (20), the half-space EH does not couple fermions at distances higher than one, similarly to what happens for unitary integrable models in equation (8). In the left plot in figure 4(a), we see that near the endpoints the only non-zero elements of the real part of the EH kernel are the nearest-neighbour couplings $k^A_{j,j+1}$ and $k^A_{j,j-1}$. The higher couplings are non-zero only in a crossover region in the middle of the interval, as expected. This behaviour is again completely analogous to what was observed in [43] for the dimerised hopping chain. The new results are given by the imaginary part, shown in the right plot in figure 4(b). We see that also the imaginary part follows the expected behaviour, with only the main diagonal k^A being significantly different from zero near the endpoints. This confirms the validity of our local conjecture in equation (20) for

J. Stat. Mech. (2024) 063102

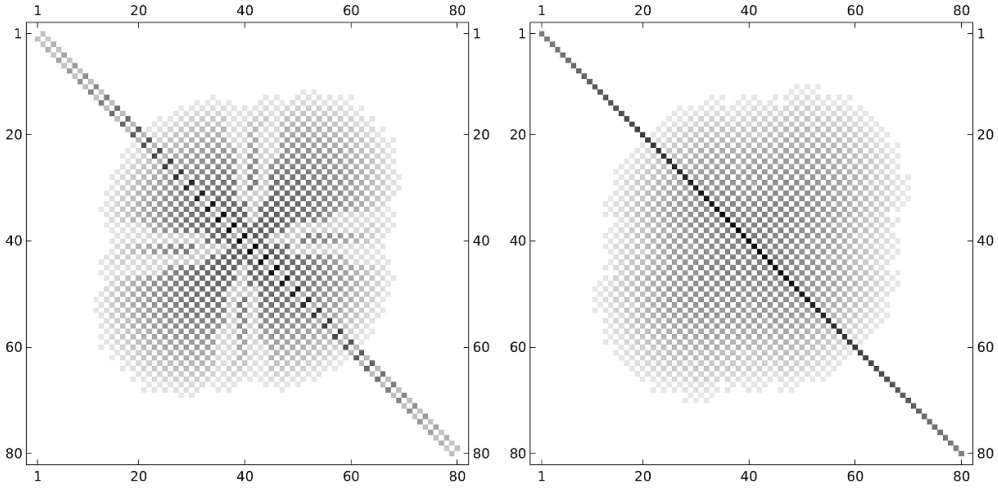

(a) Real part of the EH kernel k^A. **(b)** Imaginary part of the EH kernel k^A.

Figure 4. Matrix plot of the EH kernel k^A in the gapped phase $w - v > u$ with $w = 20$, $v = 2$ and $u = 2$, for an interval of length $\ell = 80$ in a system of length $L = 2000$. Left (Right): Absolute value of the real (imaginary) part of k^A. Consistently with the Tetel'man-Thacker behaviour (20), near the two endpoints the only non-vanishing elements of the EH are the imaginary chemical potential (main diagonal in the right plot) and the coupling between nearest-neighbours (first sub-diagonals in the left plots). The latter couplings (left) display the alternating value between the odd and even sites (see equation (20)). In the middle of the interval, the EH deviates from equation (20) and also couplings at higher distances are non-zero.

the half space EH in the non-Hermitian SSH model. We remark that this is the first observation of a Bisognano-Wichmann like behaviour in a non-Hermitian model.

Before concluding this section, we wish to comment on the proportionality constant in equation (20), i.e. the slope of the triangles in figure 3. This constant is actually related to the velocity of the excitations in the gapped model. In [43], the analogous proportionality constant in the dimerised hopping chain was computed analytically using the knowledge of the exact CTM. It would be interesting to obtain analytically the CTM in the non-Hermitian SSH model, which would refine our conjecture (20) for the half-space EH. This computation would not only allow us to predict the slope of the linearly increasing entanglement temperature, but it could also provide a quantitative understanding of the finite size oscillations of the chemical potential in figure 3(b) which are not captured by equation (20). This is however a rather involved calculation which goes beyond the scope of this work.

3.2. Entanglement Hamiltonian at the critical point

In this section we study the EH at the critical point $w - v = u$ (green square in figure 2). As discussed in section 2, at the critical point and for periodic boundary conditions, the lattice Hamiltonian (9) presents a Jordan block. Then, to treat the system numerically

J. Stat. Mech. (2024) 063102

we need to introduce a small twisting of the boundary conditions δ [73, 76]. In all the following discussion we fix $\delta = 10^{-7}$. In full analogy to the study we performed for the gapped phase in section 3.1, we compute numerically the lattice EH kernel k^A using equation (19), performing all calculations at high precision. However, at the critical point there is an additional subtlety. In [73] it was shown that at criticality all eigenvalues ν_j of the correlation matrix are real and lie outside of the interval $[0,1]$. As a consequence, the matrix appearing inside the logarithm in equation (19) has all negative eigenvalues (see also [76]). This is susceptible to numerical instabilities, giving an imaginary part of the logarithm which (unphysically) oscillates wildly between $+\mathrm{i}\pi$ and $-\mathrm{i}\pi$. In this work we always fix it to be equal to $+\mathrm{i}\pi$.

Before presenting our numerical results for the critical non-Hermitian SSH model, we would like to reiterate what occurs in the case of unitary gapless models. According to equation (5), in the vacuum of the CFT describing the continuum limit of a critical model, the EH of an interval is proportional to the energy density with a parabolic entanglement temperature $\beta(x)$ [20–23]. One could be tempted to conclude that the EH of an interval in a critical model should be proportional to the critical Hamiltonian density with the parabolic temperature in equation (5). This behaviour would in particular imply that all terms of the lattice EH that couple fermions at distances higher than those in the Hamiltonian must be negligible. However, as recognised first in [93], this is not the case, and the EH contains couplings at arbitrary distances (see also [44–46]). Moreover, when expanding the lattice fermions in the lattice spacing, all these higher couplings contribute to the continuum energy density T_{00} [94, 95]. In [94–96] it was shown that in order to recover the CFT entanglement temperature $\beta(x)$ in equation (5), it is necessary to perform a careful continuum limit which takes into account all of these higher contributions. This limiting procedure has allowed to reconstruct the CFT EH in many systems at criticality, both at finite temperature and in the ground state [94–96] and also in the presence of boundaries [95–97], in inhomogeneous and out-of-equilibrium systems [98, 99] and in higher dimensions [100]. In [97, 101] it has also been extended to the recently introduced negativity Hamiltonian [102], i.e. the logarithm of the partial transposed density matrix. On the other hand, this limit is highly dependent on the lattice model and, to date, it is only understood in the case of free massless lattice fermions and the harmonic chain.

Considering now the non-Hermitian SSH model, in figures 5 and 6, we report the numerical lattice EH, obtained from equation (19) with a choice of parameters $w = 1.5$, $v = 1$ and $u = w - v = 0.5$ and different interval lengths $\ell = 60, 100$ and 120 in a total system of length $L = 2000$. In figure 5 we plot the real part of the nearest-neighbour coupling $k^A_{j,j+1}$, divided by $(-w)$ for j even and by $(-v)$ for j odd, analogously to what we have done in the massive case. We further make the quantity dimensionless by multiplying it by $2c_S/\ell$, where c_S is the speed of sound (13) in the critical lattice model. Indeed, notice that if we reintroduce the dimensions, k^A is dimensionless, while w and v have the dimensions of an inverse time. We observe a perfect collapse for all the lengths considered. The black dashed line in figure 5 is the parabolic entanglement temperature $2\pi\beta(x)$ for unitary CFTs reported in equation (5), divided by the length of the interval ℓ. While near the endpoints we find a good agreement, we see a deviation in the middle

J. Stat. Mech. (2024) 063102

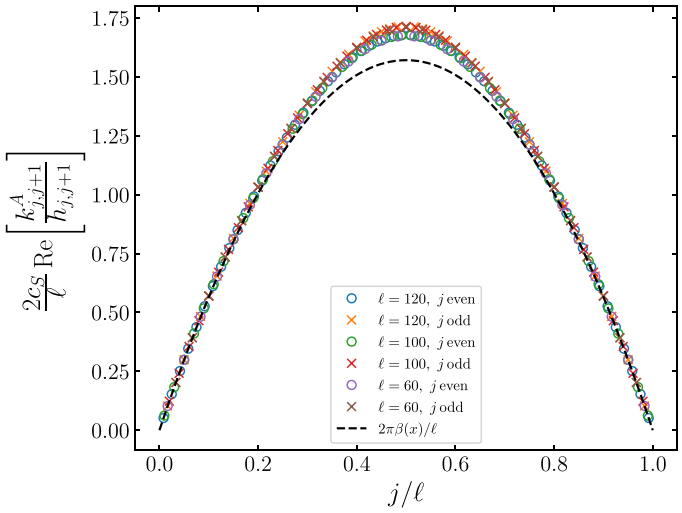

Figure 5. Real part of the ratio of the EH nearest-neighbour coupling $k^A_{j,j+1}$ with the coupling w (v) for j even (odd), rescaled by $2c_S/\ell$, where ℓ is the length of the interval and c_S is the speed of sound (13). The circles represent even sites and the crosses are odd sites. For all lengths considered we observe a perfect collapse. The black dashed parabola is the field theory prediction for the local temperature $2\pi\,\beta(x)$ in equation (5), divided by ℓ. Near the endpoints of the interval we find a very good agreement between the lattice result and the field theory. The deviation in the middle of the interval is due to the contribution of higher couplings, analogously to what happens in Hermitian lattice models.

of the interval. Similarly to what happens for unitary lattice models, the origin of this discrepancy is the presence of higher couplings which in the continuum limit give contributions to the continuum energy density. We expect that a proper continuum limit should exactly reproduce the parabola in equation (5) (as for Hermitian free fermions [94]), but this is beyond our goals.

In figure 6 we instead report the staggered imaginary chemical potential (the alternating sign with respect to figure 3(b) is due to not having divided by either u or $(-u)$). This quantity displays the most significant difference with respect to the Hermitian case. For all the lengths ℓ of the interval, at the left endpoint $j/\ell = 0$ the chemical potential takes the value $2\pi\,\mathrm{i}$ (grey dotted line), while at the right one $j\,/\ell = 1$ it vanishes. Based on this observation, we conjecture that besides the approximate parabolic result, at the critical point appears an additional term of the form

$$\sum_{j=0}^{\ell} \mu^A_{j,j}\, c^\dagger_j c_j = 2\pi\mathrm{i} \sum_{j=0}^{\ell} \left(1 - \frac{\left(j+\frac{1}{2}\right)}{\ell}\right) c^\dagger_j c_j, \tag{21}$$

i.e. a chemical potential term which interpolates linearly between $2\pi\mathrm{i}$ and 0. We remark that, differently from the parabolic entanglement temperature $\beta(x)$ in equation (5),

J. Stat. Mech. (2024) 063102

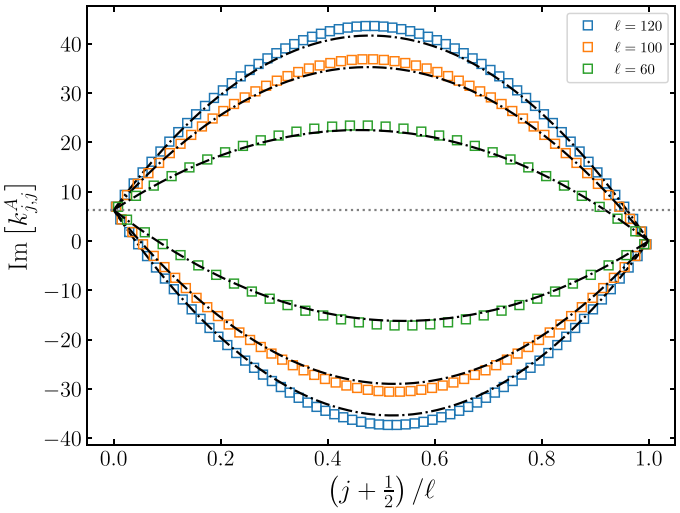

Figure 6. Imaginary chemical potential $k^A_{j,j}$ at criticality $w-v=u$ for different lengths of the interval $\ell = 60, 100$ and 120. The black dash-dotted curves are reported in equation (22) and are obtained as the sum of the naive field theory prediction for the entanglement temperature in equation (5) and of the conjectured form of the novel term in equation (21). Close to the endpoints we observe a perfect agreement which becomes slightly worse in the middle of the interval.

this novel term does not scale with the system size. In order to check equation (21), in figure 6 we compare the two curves (dash-dotted black lines)

$$\frac{\pi\,(\pm u)}{c_S}\left(\frac{(\ell-x)\,x}{\ell}\right)+2\pi\left(1-\frac{x}{\ell}\right), \tag{22}$$

with the imaginary part of the EH chemical potential term for $\ell = 60, 100$ and 120. Near the endpoints we find a perfect match for all the lengths considered, while the agreement gets slightly worse in the middle of the interval, but still acceptable.

To facilitate the comparison, we extract the part of the EH chemical potential that scales with the length of the interval by subtracting the conjectured form $\mu^A_{j,j}$ in equation (21) from the numerical result for $k^A_{j,j}$. We then divide by u for j even and by $(-u)$ for j odd to isolate the entanglement temperature and we rescale with $2c_S/\ell$ to make the quantity dimensionless. The result of this procedure is reported in figure 7. For all the values of the length considered we observe a perfect collapse, which suggests that the novel non-scaling term $\mu^A_{j,j}$ takes indeed the conjectured form (21). The black dashed curve is again the parabolic CFT prediction for the entanglement temperature in equation (5) divided by ℓ. Once again, we have a perfect agreement near the endpoints of the interval, while we observe a deviation in the middle. This deviation is always due to the presence of contributions from higher couplings.

Summing up our findings, recalling from section 2 that the critical point is described by the $c=-2$ bc-ghost CFT, we propose that the continuum limit of the difference $(k^A-\mu^A)$ must reproduce the continuum CFT EH in equation (5). Meanwhile, the

J. Stat. Mech. (2024) 063102

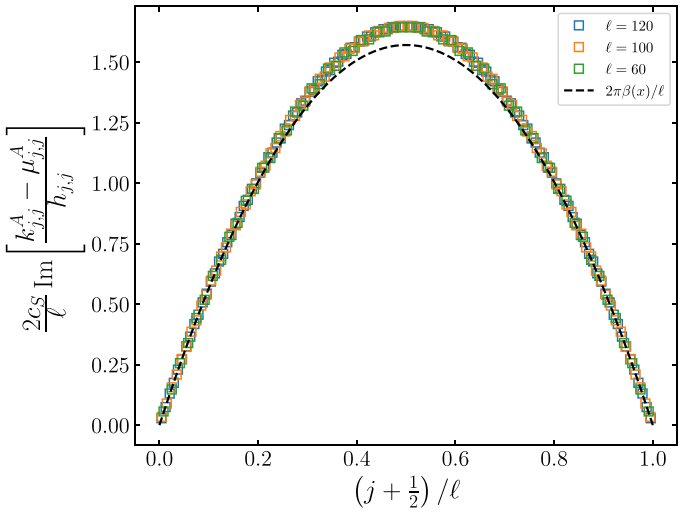

Figure 7. Imaginary part of $(k^A_{j,j}-\mu^A_{j,j})/h_{j,j}$ (i.e. the difference between the EH chemical potential and $\mu^A_{j,j}$ in equation (21), all in units of $h_{j,j}$), rescaled with $2c_S/\ell$, where c_S is the speed of sound in equation (13). We consider intervals of length $\ell = 60, 100$ and 120 in a system of total length $L = 2000$, with parameters $w = 1.5$, $v = 1$ and $u = w - v = 0.5$. For all ℓ, we observe a perfect collapse, suggesting that we have successfully isolated the scaling part. The black dashed curve is the CFT prediction for the entanglement temperature $2\pi\beta$ in equation (5) divided by ℓ. Analogously to the nearest-neighbour coupling in figure 5, the agreement is perfect at the endpoints and is slightly worse in the middle of the interval, due to the contribution of higher order couplings.

continuum limit associated with the new chemical potential term μ^A in equation (21) will yield

$$\sum_{j=0}^{\ell} \mu^A_{j,j}\, c^\dagger_j c_j \sim 2\pi\,\mathrm{i} \int_0^\ell \mathrm{d}x \left(1-\frac{x}{\ell}\right) J(x) + \text{irrelevant operators}, \tag{23}$$

where $J(x) =: cb:(x)$ is the ghost number operator. Putting all together, we conjecture that the EH of the $c = -2$ bc-ghost CFT would take the form

$$K_A = \int_0^\ell \mathrm{d}x\, \frac{x\,(\ell-x)}{\ell}\, T_{00}(x) + 2\pi\,\mathrm{i} \int_0^\ell \mathrm{d}x \left(1-\frac{x}{\ell}\right) J(x), \tag{24}$$

which is one of the main results of this paper. Comparing the proposed EH with the result for unitary CFTs in equation (5), the main difference is the presence of the imaginary term proportional to the ghost number $J(x)$. Nevertheless, since this term is again the integral of a local operator, our conjecture (24) retains a local structure. Notice that, since the conformal dimension of the ghost number operator $J(x)$ is $\Delta_J = 1$, the local weight $(1 - x/\ell)$ is dimensionless and it does not scale with the system size, as we observed on the lattice.

J. Stat. Mech. (2024) 063102

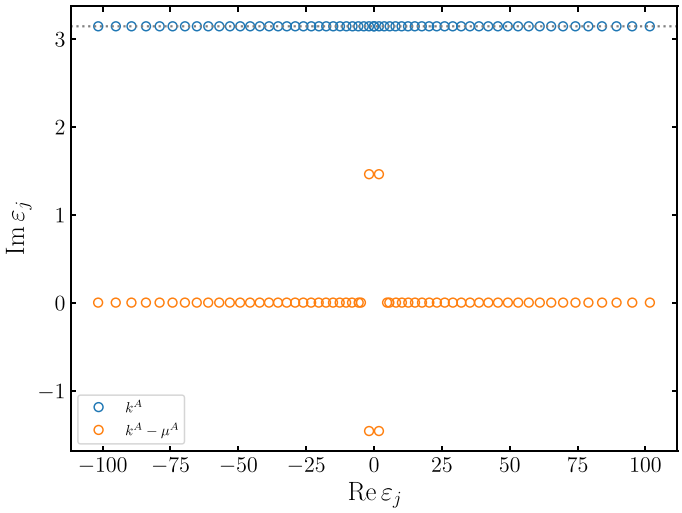

Figure 8. Spectra of the single-particle EH k^A (blue) and of the difference $(k^A - \mu^A)$ (orange), where μ^A is given by equation (21). The data are for an interval of length $\ell = 120$, in a system of size $L = 2000$, and couplings $w = 1.5$, $v = 1$ and $u = w - v = 0.5$. All eigenvalues of the EH have imaginary part equal to π (gray dotted line). Subtracting μ^A has the net effect of making almost all the eigenvalues real.

In order to understand the role played by the term μ^A in equation (21), in figure 8 we compare the single-particle entanglement spectrum, i.e. the eigenvalues of k^A, with the eigenvalues of the matrix $(k^A - \mu^A)$. All the eigenvalues ε_j of the single-particle EH (blue circles) possess an imaginary part equal to π, a feature previously identified in [76]. As already mentioned, this imaginary part is due to the fact that the eigenvalues ν_j of the correlation matrix all belong to $(-\infty, 0) \cup (1, +\infty)$, which, using equation (19), leads to [76]

$$\varepsilon_j = \log \left| \frac{1 - \nu_j}{\nu_j} \right| + \mathrm{i}\pi \,. \tag{25}$$

As discussed in section 2.2, the impact of the imaginary part in equation (25) on the many-body spectrum of the reduced density matrix is to impart an alternating sign to the eigenvalues of ρ_A depending on the charge sector, i.e. the number of ghosts, according to [76]

$$\rho_A = (-1)^{Q_A - \langle Q_A \rangle} |\rho_A| \,, \tag{26}$$

which in turn is responsible for the negative sign of the entanglement entropy. On the other hand, in figure 8 we see that the eigenvalues of $(k^A - \mu^A)$ (orange circles) are almost all real. We can therefore argue that the novel operator μ^A in equation (21) (and its continuum limit (23) in the bc-ghost CFT) is the one responsible for the alternating sign of the entanglement spectrum. Without the operator μ^A, the reduced density matrix

J. Stat. Mech. (2024) 063102

ρ_A would be positive defined and, as a consequence, the entanglement entropy would be positive too.

4. Conclusions

In this work we have have studied the ground state EH in the non-Hermitian SSH model, considering the left-right density matrix $\rho = |R\rangle\langle L|$. We studied both the topologically trivial gapped phase and the critical point. In the gapped phase, the EH assumes the typical triangular shape (see equation (20) and discussion) that was already observed in [43] for unitary integrable gapped models. Near the endpoints of the interval, the entanglement temperature grows linearly with the lattice site, according to the half-space prediction in equation (20). Remarkably, we observe that the same behaviour is true for the imaginary part of the EH. This is the first example of a lattice Bisognano-Wichmann like behaviour in a non-Hermitian model.

At the critical point, described by the bc-ghost CFT, we find a departure from the parabolic EH in equation (5) predicted by the Bisognano-Wichmann theorem for unitary CFTs. In addition to a term proportional to the energy density with a parabolic entanglement temperature, we observe a term proportional to the number operator $c_i^\dagger c_i$ with an imaginary chemical potential interpolating between $2\pi\,\mathrm{i}$ and 0, cf equation (21). This operator has a profound effect on the entanglement spectrum. As depicted in figure 8, removing the operator in equation (21) ensures that almost all the eigenvalues are real. As discussed in [76], the imaginary part of the single-particle entanglement spectrum in equation (25) is responsible for the negativeness of the entanglement entropy. If the operator in equation (21) were not present, the entanglement entropy would be positive. Based on these results, we formulate a conjecture given by equation (24) for the EH in the bc-ghost CFT. Such a conjecture consists of a term analogous to the Bisognano-Wichmann EH in equation (5) and of an imaginary chemical potential term proportional to the ghost number $J(x)$.

This paper paves the way for future investigations into the EHs of non-Hermitian models. Three open problems emerges very naturally. Firstly, in the gapped phase, it would be interesting to derive analytically the CTM. As discussed in section 3.1, this would determine the slope of the triangular entanglement temperature in figure 3 and could validate the lattice Bisognano-Wichmann behaviour. Secondly, it is desirable to analytically derive the EH at the critical point, akin to the work done for free massless fermions in [25]. Thirdly, the robustness of our findings remains uncertain, such as whether the conjectured form of the EH withstands the presence of relevant interactions. Other unexplored research directions include understanding the EH for non-Hermitian systems that lack a real Hamiltonian spectrum.

Acknowledgments

We are grateful to G Di Giulio and I Peschel for useful discussions. The authors acknowledge support from ERC under Consolidator Grant Number 771536 (NEMO).

J. Stat. Mech. (2024) 063102

F R acknowledges support from the project 'Artificially devised many-body quantum dynamics in low dimensions - ManyQLowD' funded by the MIUR Progetti di Ricerca di Rilevante Interesse Nazionale (PRIN) Bando 2022 - Grant 2022R35ZBF.

References

[1] Nielsen M A and Chuang I L 2012 *Quantum Computation and Quantum Information* (Cambridge University Press)
[2] Nishioka T, Ryu S and Takayanagi T 2009 Holographic entanglement entropy: an overview *J. Phys. A: Math. Theor.* **42** 504008
[3] Amico L, Fazio R, Osterloh A and Vedral V 2008 Entanglement in many-body systems *Rev. Mod. Phys.* **80** 517
[4] Calabrese P, Cardy J and Doyon B 2009 Entanglement entropy in extended quantum systems *J. Phys. A: Math. Theor.* **42** 500301
[5] Eisert J, Cramer M and Plenio M B 2010 Area laws for the entanglement entropy—a review *Rev. Mod. Phys.* **82** 277
[6] Laflorencie N 2016 Quantum entanglement in condensed matter systems *Phys. Rep.* **646** 1
[7] Calabrese P and Cardy J L 2004 Entanglement entropy and quantum field theory *J. Stat. Mech.* P06002
[8] Calabrese P and Cardy J 2009 Entanglement entropy and conformal field theory *J. Phys. A: Math. Theor.* **42** 504005
[9] Li H and Haldane F 2008 Entanglement spectrum as a generalization of entanglement entropy: identification of topological order in non-Abelian fractional quantum Hall effect states *Phys. Rev. Lett.* **101** 010504
[10] Calabrese P and Lefevre A 2008 Entanglement spectrum in one-dimensional systems *Phys. Rev.* A **78** 032329
[11] Alba V, Calabrese P and Tonni E 2018 Entanglement spectrum degeneracy and the Cardy formula in 1+1 dimensional conformal field theories *J. Phys. A: Math. Theor.* **51** 024001
[12] Haag R 1996 *Local Quantum Physics* (*Theoretical and Mathematical Physics*) (Springer)
[13] Witten E 2018 APS medal for exceptional achievement in research: invited article on entanglement properties of quantum field theory *Rev. Mod. Phys.* **90** 045003
[14] Dalmonte M, Eisler V, Falconi M and Vermersch B 2022 Entanglement Hamiltonians: from field theory to lattice models and experiments *Ann. Phys., Lpz.* **534** 2200064
[15] Bisognano J J and Wichmann E H 1975 On the duality condition for a Hermitian scalar field *J. Math. Phys.* **16** 985
[16] Bisognano J J and Wichmann E H 1976 On the duality condition for quantum fields *J. Math. Phys.* **17** 303
[17] Fulling S A 1973 Nonuniqueness of canonical field quantization in Riemannian space-time *Phys. Rev.* D **7** 2850
[18] Davies P C W 1975 Scalar particle production in Schwarzschild and Rindler metrics *J. Phys. A: Math. Gen.* **8** 609
[19] Unruh W G 1976 Notes on black hole evaporation *Phys. Rev.* D **14** 870
[20] Hislop P D and Longo R 1982 Modular structure of the local algebras associated with the free massless scalar field theory *Commun. Math. Phys.* **84** 71
[21] Casini H, Huerta M and Myers R C 2011 Towards a derivation of holographic entanglement entropy *J. High Energy Phys.* JHEP05(2011)036
[22] Wong G, Klich I, Zayas L A P and Vaman D 2013 Entanglement temperature and entanglement entropy of excited states *J. High Energy Phys.* JHEP12(2013)020
[23] Cardy J and Tonni E 2016 Entanglement hamiltonians in two-dimensional conformal field theory *J. Stat. Mech.* 123103
[24] Sárosi G and Ugajin T 2018 Modular Hamiltonians of excited states, OPE blocks and emergent bulk fields *J. High Energy Phys.* JHEP01(2018)012
[25] Casini H and Huerta M 2009 Reduced density matrix and internal dynamics for multicomponent regions *Class. Quantum Grav.* **26** 185005
[26] Arias R E, Casini H, Huerta M and Pontello D 2018 Entropy and modular Hamiltonian for a free chiral scalar in two intervals *Phys. Rev.* D **98** 125008
[27] Dalmonte M, Vermersch B and Zoller P 2018 Quantum simulation and spectroscopy of entanglement Hamiltonians *Nat. Phys.* **14** 827
[28] Kokail C, van Bijnen R, Elben A, Vermersch B and Zoller P 2021 Entanglement Hamiltonian tomography in quantum simulation *Nat. Phys.* **17** 936

J. Stat. Mech. (2024) 063102

[29] Kokail C, Sundar B, Zache T V, Elben A, Vermersch B, Dalmonte M, van Bijnen R and Zoller P 2021 Quantum variational learning of the entanglement Hamiltonian *Phys. Rev. Lett.* **127** 170501
[30] Zache T V, Kokail C, Sundar B and Zoller P 2022 Entanglement spectroscopy and probing the Li-Haldane conjecture in topological quantum matter *Quantum* **6** 702
[31] Joshi M K, Kokail C, van Bijnen R, Kranzl F, Zache T V, Blatt R, Roos C F and Zoller P 2023 Exploring large-scale entanglement in quantum simulation *Nature* **624** 539
[32] Peschel I and Truong T T 1987 Corner transfer matrices and conformal invariance *Z. Phys.* B **69** 385
[33] Davies B 1988 Corner transfer matrices for the Ising model *Physica* A **154** 1
[34] Truong T T and Peschel I 1989 Diagonalisation of finite-size corner transfer matrices and related spin chains *Z. Phys.* B **75** 119
[35] Peschel I, Kaulke M and Legeza ö 1999 Density-matrix spectra for integrable models *Ann. Phys., Lpz.* **8** 153
[36] Davies B 1989 On the spectrum of six-vertex corner transfer matrices *Physica* A **159** 171
[37] Frahm H and Thacker H B 1991 Corner transfer matrix eigenstates for the six vertex model *J. Phys. A: Math. Gen.* **24** 5587
[38] Tetel'man M G 1982 Lorentz group for two-dimensional integrable lattice systems *Sov. Phys. -JETP* **55** 306
[39] Thacker H B 1986 Corner transfer matrices and Lorentz invariance on a lattice *Physica* D **18** 348
[40] Ercolessi E, Evangelisti S and Ravanini F 2010 Exact entanglement entropy of the XYZ model and its sine-Gordon limit *Phys. Lett.* A **374** 2101
[41] Peschel I and Truong T T 1991 Corner transfer matrices for the Gaussian model *Ann. Phys., Lpz.* **48** 185
[42] Peschel I and Chung M-C 1999 Density matrices for a chain of oscillators *J. Phys. A: Math. Gen.* **32** 8419
[43] Eisler V, Di Giulio G, Tonni E and Peschel I 2020 Entanglement Hamiltonians for non-critical quantum chains *J. Stat. Mech.* 103102
[44] Giudici G, Mendes-Santos T, Calabrese P and Dalmonte M 2018 Entanglement Hamiltonians of lattice models via the Bisognano-Wichmann theorem *Phys. Rev.* B **98** 134403
[45] Mendes-Santos T, Giudici G, Dalmonte M and Rajabpour M A 2019 Entanglement Hamiltonian of quantum critical chains and conformal field theories *Phys. Rev.* B **100** 155122
[46] Zhang J, Calabrese P, Dalmonte M and Rajabpour M A 2020 Lattice Bisognano-Wichmann modular Hamiltonian in critical quantum spin chains *SciPost Phys. Core* **2** 007
[47] Eisler V 2024 Entanglement Hamiltonian of a nonrelativistic Fermi gas *Phys. Rev.* B **109** L201113
[48] Baxter R J 1982 *Exactly Solved Models in Statistical Mechanics* (Academic)
[49] Baxter R J 1976 Corner transfer matrices of the eight-vertex model. 1. Low-temperature expansions and conjectured properties *J. Stat. Phys.* **15** 485
[50] Baxter R J 1977 Corner transfer matrices of the eight-vertex model. 2. The Ising model case *J. Stat. Phys.* **17** 1
[51] Nishino T and Okunishi K 1997 Corner transfer matrix algorithm for classical renormalization group *J. Phys. Soc. Japan* **66** 3040
[52] Itoyama H and Thacker H B 1987 Lattice Virasoro algebra and corner transfer matrices in the Baxter eight vertex model *Phys. Rev. Lett.* **58** 1395
[53] Thacker H B and Itoyama H 1988 Integrability, conformal symmetry and noncritical Virasoro algebras *Nucl. Phys.* B **5** 9
[54] Itoyama H and Thacker H B 1989 Integrability and Virasoro symmetry of the noncritical Baxter-Ising model *Nucl. Phys.* B **320** 541
[55] Moiseyev N 2011 *Non-Hermitian Quantum Mechanics* (Cambridge University Press)
[56] Ashida Y, Gong Z and Ueda M 2021 Non-Hermitian physics *Adv. Phys.* **69** 249
[57] Bender C M and Boettcher S 1998 Real spectra in nonHermitian Hamiltonians having PT symmetry *Phys. Rev. Lett.* **80** 5243
[58] Bender C M 2015 PT-symmetric quantum theory *J. Phys.: Conf. Ser.* **631** 012002
[59] El-Ganainy R, Makris K G, Khajavikhan M, Musslimani Z H, Rotter S and Christodoulides D N 2018 Non-Hermitian physics and PT symmetry *Nat. Phys.* **14** 11
[60] Arouca R, Lee C H and Morais Smith C 2020 Unconventional scaling at non-Hermitian critical points *Phys. Rev.* B **102** 245145
[61] Arouca R, Marino E C and Morais Smith C 2022 Non-Hermitian quantum gases: a platform for imaginary time crystals *Quantum Front.* **1** 2
[62] Noble J H, Lubasch M, Stevens J and Jentschura U D 2017 Diagonalization of complex symmetric matrices: generalized Householder reflections, iterative deflation and implicit shifts *Comput. Phys. Commun.* **221** 304
[63] Feng L, El-Ganainy R and Ge L 2017 Non-Hermitian photonics based on parity–time symmetry *Nat. Photon.* **11** 752

J. Stat. Mech. (2024) 063102

[64] Miri M-A and Alù A 2019 Exceptional points in optics and photonics *Science* **363** 6422
[65] Graefe E M, Korsch H J and Niederle A E 2008 Mean-field dynamics of a non-Hermitian Bose-Hubbard dimer *Phys. Rev. Lett.* **101** 150408
[66] Rotter I 2009 A non-Hermitian Hamilton operator and the physics of open quantum systems *J. Phys. A: Math. Theor.* **42** 153001
[67] Müller M, Diehl S, Pupillo G and Zoller P 2012 Engineered open systems and quantum simulations with atoms and ions *Adv. At. Mol. Opt. Phys.* **61** 1
[68] Gopalakrishnan S and Gullans M J 2021 Entanglement and purification transitions in non-Hermitian quantum mechanics *Phys. Rev. Lett.* **126** 170503
[69] Biella A and Schiró M 2021 Many-body quantum Zeno effect and measurement-induced subradiance transition *Quantum* **5** 528
[70] Turkeshi X, Biella A, Fazio R, Dalmonte M and Schiró M 2021 Measurement-induced entanglement transitions in the quantum Ising chain: from infinite to zero clicks *Phys. Rev.* B **103** 224210
[71] Müller T, Diehl S and Buchhold M 2022 Measurement-induced dark state phase transitions in long-ranged fermion systems *Phys. Rev. Lett.* **128** 010605
[72] Turkeshi X and Schiró M 2023 Entanglement and correlation spreading in non-Hermitian spin chains *Phys. Rev.* B **107** L020403
[73] Chang P-Y, You J-S, Wen X and Ryu S 2020 Entanglement spectrum and entropy in topological non-Hermitian systems and nonunitary conformal field theory *Phys. Rev. Res.* **2** 033069
[74] Holzhey C, Larsen F and Wilczek F 1994 Geometric and renormalized entropy in conformal field theory *Nucl. Phys.* B **424** 443
[75] Tu Y-T, Tzeng Y-C and Chang P-Y 2022 Rényi entropies and negative central charges in non-Hermitian quantum systems *SciPost Phys.* **12** 194
[76] Fossati M, Ares F and Calabrese P 2023 Symmetry-resolved entanglement in critical non-Hermitian systems *Phys. Rev.* B **107** 205153
[77] Lieu S 2018 Topological phases in the non-Hermitian Su-Schrieffer-Heeger model *Phys. Rev.* B **97** 045106
[78] Friedan D, Martinec E J and Shenker S H 1986 Conformal invariance, supersymmetry and string theory *Nucl. Phys.* B **271** 93
[79] Guruswamy S and Ludwig A W W 1998 Relating c $<$ 0 and c $>$ 0 conformal field theories *Nucl. Phys.* B **519** 661
[80] Kausch H G 1995 Curiosities at $c = -2$ (arXiv:hep-th/9510149)
[81] Kausch H G 2000 Symplectic fermions *Nucl. Phys.* B **583** 513
[82] Di Francesco P, Mathieu P and Senechal D 1997 *Conformal Field Theory* (*Graduate Texts in Contemporary Physics*) (Springer)
[83] Brody D C 2013 Biorthogonal quantum mechanics *J. Phys. A: Math. Theor.* **47** 035305
[84] Couvreur R, Jacobsen J L and Saleur H 2017 Entanglement in nonunitary quantum critical spin chains *Phys. Rev. Lett.* **119** 040601
[85] Dupic T, Estienne B and Ikhlef Y 2018 Entanglement entropies of minimal models from null-vectors *SciPost Phys.* **4** 031
[86] Herviou L, Regnault N and Bardarson J H 2019 Entanglement spectrum and symmetries in non-Hermitian fermionic non-interacting models *SciPost Phys.* **7** 069
[87] Tang W, Verstraete F and Haegeman J 2023 Matrix product state fixed points of non-Hermitian transfer matrices (arXiv:2311.18733)
[88] Chung M-C and Peschel I 2001 Density-matrix spectra of solvable fermionic systems *Phys. Rev.* B **64** 064412
[89] Peschel I 2003 Calculation of reduced density matrices from correlation functions *J. Phys. A: Math. Gen.* **36** L205
[90] Peschel I and Eisler V 2009 Reduced density matrices and entanglement entropy in free lattice models *J. Phys. A: Math. Theor.* **42** 504003
[91] The `mpmath` Development Team 2023 `mpmath`: a Python library for arbitrary-precision floating-point arithmetic (version 1.3.0) (available at: http://mpmath.org/)
[92] Alba V, Haque M and Läuchli A M 2012 Boundary-locality and perturbative structure of entanglement spectra in gapped systems *Phys. Rev. Lett.* **108** 227201
[93] Arias R, Blanco D, Casini H and Huerta M 2017 Local temperatures and local terms in modular Hamiltonians *Phys. Rev.* D **95** 065005
[94] Eisler V, Tonni E and Peschel I 2019 On the continuum limit of the entanglement Hamiltonian *J. Stat. Mech.* 073101

J. Stat. Mech. (2024) 063102

[95] Eisler V, Tonni E and Peschel I 2022 Local and non-local properties of the entanglement Hamiltonian for two disjoint intervals *J. Stat. Mech.* 083101
[96] Di Giulio G and Tonni E 2020 On entanglement hamiltonians of an interval in massless harmonic chains *J. Stat. Mech.* 033102
[97] Rottoli F, Murciano S, Tonni E and Calabrese P 2023 Entanglement and negativity Hamiltonians for the massless Dirac field on the half line *J. Stat. Mech.* 013103
[98] Rottoli F, Scopa S and Calabrese P 2022 Entanglement Hamiltonian during a domain wall melting in the free Fermi chain *J. Stat. Mech.* 063103
[99] Bonsignori R and Eisler V 2024 Entanglement Hamiltonian for inhomogeneous free fermions (arXiv:2403.14766)
[100] Javerzat N and Tonni E 2022 On the continuum limit of the entanglement Hamiltonian of a sphere for the free massless scalar field *J. High Energy Phys.* JHEP02(2022)086
[101] Rottoli F, Murciano S and Calabrese P 2023 Finite temperature negativity Hamiltonians of the massless Dirac fermion *J. High Energy Phys.* JHEP06(2023)139
[102] Murciano S, Vitale V, Dalmonte M and Calabrese P 2022 Negativity Hamiltonian: an operator characterization of mixed-state entanglement *Phys. Rev. Lett.* **128** 140502

J. Stat. Mech. (2024) 063102